THE JOURNAL OF PHYSICAL CHEMISTRY Letters

Letter

pubs.acs.org/JPCL

# X-ray Photoelectron Spectroscopy of Isolated Nanoparticles

Olivier Sublemontier,*[,⊥,†] Christophe Nicolas,[⊥,‡] Damien Aureau,[§] Minna Patanen,[‡] Harold Kintz,[†] Xiaojing Liu,[‡] Marc-André Gaveau,[†] Jean-Luc Le Garrec,[∥] Emmanuel Robert,[‡] Flory-Anne Barreda,[†,‡] Arnaud Etcheberry,[§] Cécile Reynaud,[†] James B. Mitchell,[∥] and Catalin Miron*[,‡]

[†]CEA/IRAMIS/Laboratoire Francis Perrin, URA 2453, 91191 Gif-sur-Yvette, France

[‡]Synchrotron SOLEIL, L'Orme des Merisiers, Saint—Aubin, BP 48, 91192 Gif-sur-Yvette Cedex, France

[§]Institut Lavoisier de Versailles, Université Versailles—St Quentin, UMR CNRS 8180, 78035 Versailles, France

[∥]Institut de Physique de Rennes, Université Rennes 1, 35042 Rennes, France

Supporting Information

**ABSTRACT:** X-ray photoelectron spectroscopy (XPS) is a very efficient and still progressing surface analysis technique. However, when applied to nano-objects, this technique faces drawbacks due to interactions with the substrate and sample charging effects. We present a new experimental approach to XPS based on coupling soft X-ray synchrotron radiation with an in-vacuum beam of free nanoparticles, focused by an aerodynamic lens system. The structure of the $Si/SiO_2$ interface was probed without any substrate interaction or charging effects for silicon nanocrystals previously oxidized in ambient air. Complete characterization of the surface was obtained. The Si 2p core level spectrum reveals a nonabrupt interface.

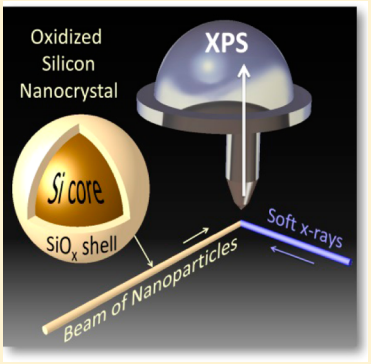


**SECTION:** Surfaces, Interfaces, Porous Materials, and Catalysis

The ability of X-ray photoelectron spectroscopy (XPS) to provide information on the local bonding environment of a given species makes it an essential tool for understanding the surface chemistry of materials.[1,2] Thereby, the Si 2p level analysis of an oxidized silicon wafer by XPS readily reveals the oxidation states of silicon at the surface.[3] It has also been demonstrated to be a unique tool for characterizing the surface[4,5] and bulk[6] chemical structure of nanoparticles. However, data collected from nano-objects often suffer from interpretation difficulties whenever samples are deposited on a substrate.[5,7] New experiments based on free nanoparticles interacting with photons are currently considered.[8,9] Here, we present a new experimental approach of XPS combining soft X-ray synchrotron radiation with an in-vacuum beam of isolated nanoparticles focused by an aerodynamic lens system. As a proof of concept, the structure of the $Si/SiO_2$ interface is probed for silicon nanocrystals (Si-NCs) previously oxidized in ambient air.

A beam of isolated nanoparticles crosses synchrotron radiation under high vacuum conditions, so that the interaction between a particle and the soft X-rays is well defined both spatially and temporally. A diphasic flow composed of an inert carrier gas and the sample in aerosol form is produced by atomization of a suspension of nanoparticles. The nanoaerosol mobility diameter and number density are measured online using a commercial scanning mobility particle sizer (SMPS). An aerodynamic lens system (ADLS) produces a focused, continuously renewable, nanoparticle beam under vacuum from the aerosol stream at atmospheric pressure. This is achieved by carrying the nanoaerosol flow through a 200 $\mu$m limiting entrance orifice followed by a series of four compartments separated by diaphragms. The geometry of the ADLS is identical to the design proposed by Jayne et al.[10] It is part of a dedicated multipurpose source chamber available on the PLEIADES beamline at the French national synchrotron radiation facility SOLEIL.[11] The experimental arrangement is shown in Figure 1.

The trajectories of the nanoaerosols get closer and closer to the axis as they move through the lens and the beam is then focused at a distance of between a few centimeters and several tens of centimeters from the ADLS outlet. The nanoparticle beam passes entirely through a 1.5 mm diameter skimmer and emerges into a high vacuum region before crossing the soft X-ray beam. The pressure in the interaction chamber is maintained at around $1 \times 10^{-6}$ mbar.

The sample of Si-NCs was first synthesized by laser pyrolysis.[12] About 500 mg of dry powder of Si-NCs was synthesized for the experiments. The sample was oxidized after synthesis by exposure to ambient air over 2 months, then dispersed in ethanol and shaken ultrasonically just prior to the

**Received:** July 21, 2014
**Accepted:** September 14, 2014
**Published:** September 15, 2014

   dx.doi.org/10.1021/jz501532c | J. Phys. Chem. Lett. 2014, 5, 3399−3403

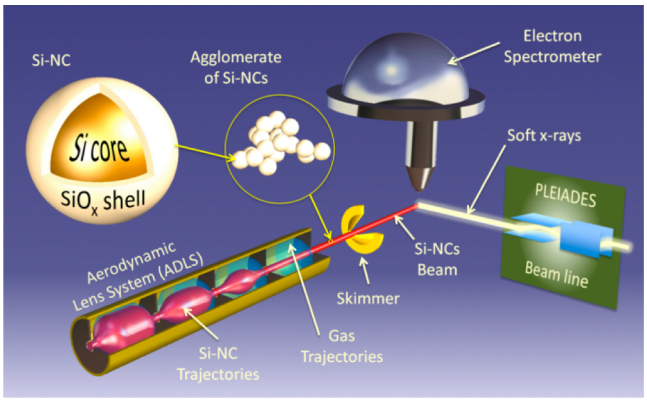


**Figure 1.** Experimental arrangement. A beam of isolated Si-NCs crosses the soft X-ray beam. The trajectories of the nanoaerosols are represented in red and the atom trajectories of the carrier gas, Ar, in the ADLS are shown in blue. The Si-NC beam passes through a 1.5 mm diameter skimmer before crossing the soft X-ray beam. Photoelectron kinetic energy spectra are recorded using a VG-Scienta R4000 spectrometer.

experiments. It was characterized using high resolution transmission electron microscopy (HRTEM, see Supporting Information). The primary particle size was 14 ± 2 nm, including the thin amorphous oxide layer that appeared at the surface of the particles during air exposure (see Supporting Information). Fluid dynamics calculations have shown that the ADLS has the ability to focus high-density spherical nanoparticles down to about 40 nm in diameter.[13] For smaller particles, Brownian motion significantly impacts their trajectories in the ADLS and at its immediate outlet, leading to a divergent beam that provides a too low particle density for spectroscopic studies using synchrotron radiation. However, an efficient way to overcome this difficulty is to get the nanoparticles deliberately in agglomerated form in the beam, but still with independent primary particles. This can be achieved by controlling the Si-NC concentration in the atomized suspension. For this purpose, the mass concentration was set at 1g/l in ethanol. The size of the nanoaerosols after atomization was then stable with time and constantly monitored to have a mobility diameter of $D_m$ = 150 nm, independent of the ultrasonic treatment time. This mobility diameter is compatible with the ADLS focusing abilities and results from diffusion-limited agglomeration of primary Si-NCs occurring at the atomization stage of the suspension and in the streamline up to the ADLS outlet. It corresponds to an average number of 154 primary particles per agglomerate.[14] We measured the beam profile of agglomerated Si-NCs obtained with the ADLS using laser-induced breakdown detection (unpublished results). We have demonstrated aerodynamic focusing on an 82 $\mu$m beam diameter (see Supporting Information). Considering the geometrical cross section of the agglomerates[15] and their velocity[13] on the one hand, and the soft X-ray photon intensity on the other hand, the probability for a single Si-NC to be doubly or multiply ionized in the interaction region is negligible. As the sample is continuously renewable, no charge effect is then expected in our experiments.

Soft X-ray photoelectron spectroscopy experiments were carried out at the ultrahigh resolution[16,17] soft X-ray PLEIADES beamline (9−1000 eV) at SOLEIL. The photoelectron spectra were recorded above the Si 2p threshold using a 30° wide-angle lens, VG-Scienta R4000 electron energy analyzer. The incident photon energy was 158 eV, leading to photoelectrons with about 50 eV of kinetic energy and, thus, electron escape depths of around 0.63 nm in $SiO_2$ and 0.34 nm in Si, as estimated from previous measurements.[3] These values are much smaller than those for laboratory tabletop XPS instruments, which are, for instance, 2.96 and 2.41 nm for $SiO_2$ and Si, respectively, when using Mg K$\alpha$ X-rays.[18] As the depth analyzed is very thin, the effects from elastic scattering are neglected.[19] The electron attenuation length is then assumed equivalent to the electron mean free path. The photon energy resolution was chosen to be 214 meV, and the electron kinetic energy resolution was 100 meV.

A high-resolution SR-XPS spectrum on isolated Si-NCs is given in Figure 2. The data collection time was about 3 h. For

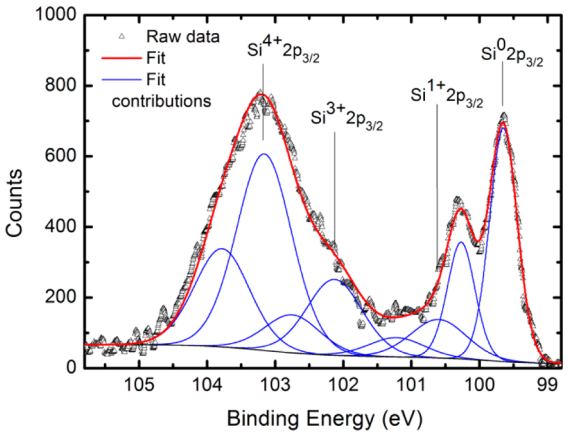


**Figure 2.** Si 2p photoelectron spectrum of isolated Si-NCs. The empty triangles represent the raw data and the red curve is a fit taking into account the different fitted oxidation state contributions (blue curves). The positions of Si $2p_{3/2}$ for $Si^0$, $Si^{1+}$, $Si^{3+}$, and $Si^{4+}$ are pointed out. The contribution from $Si^{2+}$ was found to be very low (see text).

each contribution, the intensity ratio of 2 between the two spin−orbit components and their constant splitting of 0.61 eV was taken into account.[3] A Shirley-type background was used. The quality of the fit is satisfactory according to the statistical dispersion of the raw data. The binding energy scale was tentatively adopted by subtracting from the calibrated photon energy, the measured kinetic energy and the work function of bulk Si that was previously measured to be 4.87 eV.[20] As the size of the primary particles is relatively large (14 nm), we do not expect any size dependence of the Si 2p core level shift due to strain effects, as reported for Si-NCs smaller than 4 nm.[21] Nor do we expect size-related changes in the electronic properties that may have an impact on the work function for sizes below 5 nm.[22] The argument to use the work function for bulk Si in the present case is supported by the coincidence of the Si $2p_{3/2}$ line position in our spectra and the one that is most frequently reported in the literature for bulk Si.[3] As discussed previously, no charge effect is expected. The energy scale is then free from ghost shifts due to this effect.

The relative intensity measured for the oxidation states of Si, denoted by $Si^0$, $Si^{1+}$, $Si^{2+}$, $Si^{3+}$, and $Si^{4+}$, are respectively 0.67, 0.27, 0, 0.56, and 1, given by the fitting procedure shown in Figure 2. The binding energies relative to the $Si^0$ positions for each Si $2p_{3/2}$ contribution are respectively 0.95, 2.48, and 3.51 eV for $Si^{1+}$, $Si^{3+}$, and $Si^{4+}$. The line positions are kept free in the fitting process and are found to appear at values consistent with


dx.doi.org/10.1021/jz501532c | J. Phys. Chem. Lett. 2014, 5, 3399−3403

those obtained for bulk surfaces of oxidized Si wafers, with the exception of the $Si^{4+}$ relative position.[3] The latter was found 3.51 eV above $Si^0$, compared to 3.90 eV measured on a clean Si(100) bulk surface. This difference is explained by the oxide thickness difference between the two measurements, which was previously demonstrated to have a significant impact on the $Si^{4+}$ contribution position for oxide films thinner than 1 nm.[23] The relative intensity contributions from intermediate oxidation states $Si^{1+}$ and $Si^{3+}$ are significant, in agreement with previous observations inferring a nonabrupt interface.[24] However, the oxidation state distribution is different from previous studies on Si-NCs grown on substrates.[7] It is also different from suboxide synchrotron radiation analysis at the $Si/SiO_2$ interface of different crystal orientation surfaces on Si wafers.[3] In these three cases, the $Si^{2+}$ contribution was not negligible, contrary to our current observations.

The thickness $d$ of the oxide shell is calculated in the case of planar surfaces by using the following equation[25] for photoelectrons resulting from nonoxidized Si and a unique oxide state

$$d = L \cdot \ln\left(1 + \frac{I_{SiO_x}}{I_{Si}} \cdot \frac{I_{Si}^{\infty}}{I_{SiO_x}^{\infty}}\right)$$

Here, $L$ is the attenuation length of photoelectrons from the nonoxidized and the oxidized regions in the oxide layer, $I_{SiO_x}$ and $I_{Si}$ are the measured intensities of the oxide and nonoxidized Si, respectively. $I_{SiO_x}$ was calculated by taking into account the relative amount of Si in each oxide subpopulation $I_{Si^{1+}}$, $I_{Si^{2+}}$, $I_{Si^{3+}}$ and $I_{Si^{4+}}$ with nearly pure $Si^{4+}$ as a reference

$$I_{SiO_x} = 0.25I_{Si^{1+}} + 0.5I_{Si^{2+}} + 0.75I_{Si^{3+}} + I_{Si^{4+}}$$

$I_{SiO_x}^{\infty}$ and $I_{Si}^{\infty}$ are the calculated intensities from bulk materials, respectively. We assume the approximation of a constant attention length in the oxide layer (equal to the attenuation length in $SiO_2$). With $L$ = 0.63 nm and a value of $(I_{Si}^{\infty})/(I_{SiO_x}^{\infty})$ = 0.83 at 158 eV photon energy,[3] a value of 0.66 nm is thus found as an apparent thickness assuming the sample to be ideally planar. The real sample is an isolated agglomerate of primary particles, and so the general sample surface is actually made up of spheres. The simple flat layer calculation thus overestimates the thickness. The determination of the overlayer thickness on nonplanar samples has previously been addressed in detail, and a practical approach is to multiply the apparent planar thickness by a geometrical correction term, or topo factor,[26] to calculate the conformal thickness. Different correction factors are proposed for spherical or cylindrical samples. If we assume that our sample is made up of 14 nm monodisperse spheres, equally surface-oxidized, and if we consider an attenuation length of less than 1 nm with 158 eV photon energy, then a constant multiplying topo factor of 0.67 is acceptable within a 10% error.[26] Furthermore, the single sphere approximation was found to be valid in the case of uncorrelated spatial primary particle coordinates,[27] which is the case in an isolated fractal-like agglomerate. A first estimation of the oxide thickness layer is then 0.44 nm. The corresponding error bar is estimated to be ±0.1 nm, according to measurement uncertainties and approximations in the determination of the $(I_{Si}^{\infty})/(I_{SiO_x}^{\infty})$ ratio. This oxide layer thickness obtained by XPS on isolated particles is far more accurate than HRTEM estimations[18] (see Supporting Information). However, both estimations are consistent.

A saturation phenomenon of the native oxide shell thickness as a function of the size of the Si-NCs was previously observed by HRTEM.[28] This self-limited oxidation process depends linearly on size. Smaller oxide shell thicknesses are found for smaller nanoparticles. This phenomenon is related to the lattice deviation from the bulk spacing arising upon oxidation, which is dependent on size in the range from 5 to 35 nm. The expected oxide thickness saturation upon native oxidation under ambient air is around 1.5 nm for 14 nm Si-NCs. As the total oxide thickness of our sample is estimated to be 0.44 ± 0.1 nm after 2 months of native oxidation, the oxidation process appears to be incomplete. This argues for a relatively low contribution of the stoichiometric oxide layer in the photoelectron spectrum compared to those for intermediate oxidation states.

XPS on supported, stacked samples of nano-objects is widely used. It should now take into account precautions concerning the specific geometry of the sample[26] when quantitative data are sought. The influence of interactions between the sample and the substrate is difficult to predict, or to discriminate afterward. Studies of supported Si-NCs were previously conducted, either by XPS or by SR-XPS.[7] In the latter study, a significant broadening of all contributions (fwhm) was observed for Si-NCs compared to a bulk surface in the same analysis conditions and with the same oxidation treatment. The interpretation is not obvious and several effects were considered to explain this broadening. Calculations support the existence of a large size-dependent stress at the surface of oxidized Si-NCs that may induce structural disorder.[29] Nevertheless, it is not possible to exclude interactions with the substrate, as the Si-NCs were grown on it. XPS on isolated (nonsupported) nanoparticles is then fully relevant to access, directly observe, and discriminate the effects that may specifically be induced by nanostructuration of matter, avoiding any interaction with a substrate. The experimental technique should be applicable to a large range of other nano-objects including functionalized nanoparticles.

## EXPERIMENTAL METHODS

The synthesis of Si-NCs is performed in the gas phase by laser pyrolysis. A $CO_2$ high-power laser beam interacts with gaseous $SiH_4$ diluted in He at 150 mbars. Collision processes decompose $SiH_4$, following vibrational excitation during the interaction with the laser. As in most gas-phase processes, the nanoparticles synthesized by laser pyrolysis are in an agglomerated form. For this study, the average size of primary particles is 14 nm with a relative size distribution width of less than ±15%. The sample was oxidized after synthesis by exposure to ambient air over 2 months, then dispersed in ethanol and treated by ultrasound just before the experiments. The suspension appeared to be stable for several hours but was refreshed anyway after a maximum of 4 h of data collection. The mass concentration was set at 1g/L. The agglomerates were easily broken by ultrasonic postsynthesis treatment of the suspensions of Si-NCs in ethanol. The agglomerate size evolution in the suspension was monitored using dynamic light scattering (DLS) as a function of the treatment time in a low concentration solution in ethanol (0.01 g/L). An average size close to the primary particle size was obtained after 15 min of ultrasonic treatment. The agglomerates resulting from the synthesis process are then composed of weakly bonded, independent nanocrystals. The atomization of the suspension


dx.doi.org/10.1021/jz501532c | J. Phys. Chem. Lett. 2014, 5, 3399−3403

is performed by a commercial setup (Atomizer model 3076, TSI Inc.). The nanoaerosol mobility diameter and number density are measured online with a commercial scanning mobility particle sizer, composed of a differential mobility analyzer, model 3081, and a condensation particle counter, model 3786, TSI Inc.

## ■ ASSOCIATED CONTENT

### Supporting Information

High resolution transmission electron microscopy study of the sample; nanoparticle beam profile measurement; control of the sample state during SR-XPS; details of synchrotron radiation photoelectron spectroscopy; XPS fitting procedure. This material is available free of charge via the Internet at http://pubs.acs.org.

## ■ AUTHOR INFORMATION


### Corresponding Authors

*olivier.sublemontier@cea.fr.

*catalin.miron@synchrotron-soleil.fr.

### Author Contributions

[⊥](O.S., C.N.) These authors contributed equally to this work.


### Notes

The authors declare no competing financial interest.

## ■ ACKNOWLEDGMENTS

The experiment has been performed at the PLEIADES beamline at the SOLEIL Synchrotron (Proposal No. 20110423). The development of the MPSC has received funding from the Agence Nationale de la Recherche (ANR) under Grant No. ANR-07-NANO-0031. The LIBD measurements have received financial support from The RTRA Triangle de la Physique under Grants No. 2011-082T and 2013-0293T. The authors are grateful to J.N. Rouzaud from Laboratoire de Géologie de l'ENS for HRTEM micrographs. C.M. acknowledges the European COST action CM1204-XUV/X-ray light and fast ions for ultrafast chemistry (XLIC).

## ■ REFERENCES


(1) Siegbahn, K. Electron Spectroscopy for Atoms, Molecules, and Condensed Matter. *Science* **1982**, *217*, 111−21.

(2) Bernardi, F.; Fecher, G. H.; Alves, M. C. M.; Morais, J. Unraveling the Formation of Core−Shell Structures in Nanoparticles by S-XPS. *J. Phys. Chem. Lett.* **2010**, *1*, 912−917.

(3) Himpsel, F. J.; McFeely, F. R.; Taleb-Ibrahimi, A.; Yarmoff, J. A. Microscopic Structure of the Si/$SiO_2$ Interface. *Phys. Rev. B* **1988**, *38*, 6084.

(4) Baer, D. R.; Gaspar, D. J.; Nachimuthu, P.; Techane, S. D.; Castner, D. G. Application of Surface Chemical Analysis Tools for Characterization of Nanoparticles. *Anal. Bioanal. Chem.* **2010**, *396*, 983−1002.

(5) Baer, D. R.; Engelhard, M. H. XPS Analysis of Nanostructured Materials and Biological Surfaces. *J. Electron Spectrosc. Relat. Phenom.* **2010**, *178−179*, 415−432.

(6) Sarma, D. D.; Santra, P. K.; Mukherjee, S.; Nag, A. X-ray Photoelectron Spectroscopy: A Unique Tool To Determine the Internal Heterostructure of Nanoparticles. *Chem. Mater.* **2013**, *25*, 1222−1232.

(7) Renault, O.; Marlier, R.; Gely, M.; De Salvo, B.; Baron, T.; Hansson, M.; Barrett, N. T. Synchrotron Radiation X-ray Photoelectron Spectroscopy of Si Nanocrystals Grown onto $Al_2O_3$/Si Surfaces. *Appl. Phys. Lett.* **2005**, *87*, 163119.

(8) Meinen, J.; Khasminskaya, S.; Eritt, M.; Leisner, T.; Antonsson, E.; Langer, B.; Rühl, E. Core Level Photoionization on Free Sub-10-nm Nanoparticles Using Synchrotron Radiation. *Rev. Sci. Instrum.* **2010**, *81*, 085107.

(9) Xiong, W.; Hickstein, D. D.; Schnitzenbaumer, K. J.; Ellis, J. L.; Palm, B. B.; Keister, K. E.; Ding, C.; Miaja-Avila, L.; Dukovic, G.; Jimenez, J. L.; et al. Photoelectron Spectroscopy of CdSe Nanocrystals in the Gas Phase: A Direct Measure of the Evanescent Electron Wave Function of Quantum Dots. *Nano Lett.* **2013**, *13*, 2924.

(10) Jayne, J. T.; Leard, D. C.; Zhang, X.; Davidovits, P.; Smith, K. A.; Kolb, C. E.; Worsnop, D. R. Development of an Aerosol Mass Spectrometer for Size and Composition Analysis of Submicron Particles. *Aerosol Sci. Technol.* **2000**, *33*, 37.

(11) Lindblad, A.; Söderström, J.; Nicolas, C.; Robert, E.; Miron, C. A Multi-Purpose Source Chamber at the PLEIADES Beamline at SOLEIL for Spectroscopic Studies of Isolated Species: Cold Molecules, Clusters and Nanoparticles. *Rev. Sci. Instrum.* **2013**, *84*, 113105.

(12) Sublemontier, O.; Kintz, H.; Lacour, F.; Paquez, X.; Maurice, V.; Leconte, Y.; Porterat, D.; Herlin-Boime, N. Synthesis and On-line Size Control of Silicon Quantum Dots. *KONA Powder Part. J.* **2011**, *29*, 236.

(13) Wang, X.; Gidwani, A.; Girshick, S. L.; McMurry, P. H. Aerodynamic Focusing of Nanoparticles: II. Numerical Simulation of Particle Motion Through Aerodynamic Lenses. *Aerosol Sci. Technol.* **2005**, *39*, 624−636.

(14) Sorensen, C. M. The Mobility of Fractal Aggregates: A Review. *Aerosol Sci. Technol.* **2011**, *45*, 765−779.

(15) Köylü, Ü. Ö.; Faeth, G. M.; Farias, T. L.; Carvalho, M. G. Fractal and Projected Structure Properties of Soot Aggregates. *Combust. Flame* **1995**, *100*, 621−633.

(16) Travnikova, O.; Liu, J. C.; Lindblad, A.; Nicolas, C.; Söderström, J.; Kimberg, V.; Gel'mukhanov, F.; Miron, C. Circularly Polarized X Rays: Another Probe of Ultrafast Molecular Decay Dynamics. *Phys. Rev. Lett.* **2010**, *105*, 233001.

(17) Kimberg, V.; Lindblad, A.; Söderström, J.; Travnikova, O.; Nicolas, C.; Sun, Y. P.; Gel'mukhanov, F.; Kosugi, N.; Miron, C. Single-Molecule X-Ray Interferometry: Controlling Coupled Electron-Nuclear Quantum Dynamics and Imaging Molecular Potentials by Ultrahigh-Resolution Resonant Photoemission and Ab Initio Calculations. *Phys. Rev. X* **2013**, *3*, 011017.

(18) Seah, M. P.; Spencer, S. J. Ultrathin $SiO_2$ on $Si^{IV}$. Intensity Measurement in XPS and Deduced Thickness Linearity. *Surf. Interface Anal.* **2003**, *35*, 515−524.

(19) Seah, M. P.; Gilmore, I. S. Simplified Equations for Correction Parameters for Elastic Scattering Effects in AES and XPS and Attenuation Lengths. *Surf. Interface Anal.* **2001**, *31*, 835.

(20) Sebenne, C.; Bolmont, D.; Guichar, G.; Balkanski, M. Surface States from Photoemission Threshold Measurements on a Clean, Cleaved, Si (111) surface. *Phys. Rev. B* **1975**, *12*, 3280.

(21) Kim, S.; Kim, M. C.; Choi, S. H.; Kim, K. J.; Hwang, H. N.; Hwang, C. C. Size Dependence of Si 2p Core-level Shift at Si Nanocrystal/$SiO_2$ interfaces. *Appl. Phys. Lett.* **2007**, *91*, 103113.

(22) Buuren, T.; van Dinh, L.; Chase, L.; Siekhaus, W.; Terminello, L. Changes in the Electronic Properties of Si Nanocrystals as a Function of Particle Size. *Phys. Rev. Lett.* **1998**, *80*, 3803.

(23) Joong Kim, K.; Park, K. T.; Lee, J. W. Thickness Measurement of $SiO_2$ Films Thinner than 1 nm by X-ray Photoelectron Spectroscopy. *Thin Solid Films* **2006**, *500*, 356.

(24) Rochet, F.; Poncey, C.; Dufour, G.; Roulet, H.; Guillot, C.; Sirotti, F. Suboxides at the Si/$SiO_2$ Interface: a Si 2p Core Level Study with Synchrotron Radiation. *J. Non-Cryst. Solids* **1997**, *216*, 148.

(25) Hill, J. M.; Royce, D. G.; Fadley, C. S.; Wagner, L.F. J. Properties of Oxidized Silicon as Determined by Angular-Dependent X-ray Photoelectron Spectroscopy. *Chem. Phys. Lett.* **1976**, *44*, 225−231.

(26) Shard, A. G. A Straightforward Method for Interpreting XPS Data from Core−Shell Nanoparticles. *J. Phys. Chem. C* **2012**, *116*, 16806.

(27) Werner, W. S. M.; Chudzicki, M.; Smekal, W.; Powell, C. Interpretation of Nanoparticle X-ray Photoelectron Intensities. *J. Appl. Phys. Lett.* **2014**, *104*, 243106.
(28) Hofmeister, H.; Huisken, F.; Kohn, B. Lattice Contraction in Nanosized Silicon Particles Produced by Laser Pyrolysis of Silane. *Eur. Phys. J. D* **1999**, *9*, 137−140.
(29) Dalla Torre, J.; Bocquet, J.-L.; Limoge, Y.; Crocombette, J.-P.; Adam, E.; Martin, G.; Baron, T.; Rivallin, P.; Mur, P. Study of Self-limiting Oxidation of Silicon Nanoclusters by Atomistic Simulations. *J. Appl. Phys.* **2002**, *92*, 1084.